IEEE Access
Multidisciplinary | Rapid Review | Open Access Journal

Received February 6, 2021, accepted February 22, 2021, date of publication February 24, 2021, date of current version April 2, 2021.

*Digital Object Identifier 10.1109/ACCESS.2021.3062188*

# Impact of Commutation Failure Preventions on HVDC System Based on a Multi-Index Value Set Approach

**MINQUAN CHEN, ZHUORAN KANG, DEQIANG GAN, (Senior Member, IEEE), AND HAO WU, (Member, IEEE)**
College of Electrical Engineering, Zhejiang University, Hangzhou 310027, China

Corresponding author: Hao Wu (eewuhao@zju.edu.cn)

This work was supported in part by the Key Project of Smart Grid Technology and Equipment of National Key Research and Development Plan of China under Grant 2016YFB0900600, and in part by the State Grid Corporation of China under Grant 5100-201999337A-0-0-00.

**ABSTRACT** This paper proposes a systematic method, based on rational approximation and value set approach, to unravel the impact of commutation failure preventions (CFPREVs) on HVDC system dynamics. First, some output variables in HVDC system dynamics are identified as performance indices, it is shown that these indices are rational functions of CFPREVs parameters. Then a numerical approximation method is used to determine the coefficients of the rational functions which describe the analytical relationship between the suggested performance indices and parameters. To help understand the connotation of the obtained expressions, a multi-index value set approach, which exploits the power of geometry and graphics, is described in detail. Finally, the results of the rational approximation and value set approach are reported.

**INDEX TERMS** Commutation failure prevention, multi-index value set, multi-parameter analysis, rational approximation.

## I. INTRODUCTION

High Voltage Direct Current (HVDC) system [1] is a useful technology for transmitting a large amount of electric power over distance. It is well-known, however, that a HVDC system is inherently vulnerable to voltage drops caused by AC network faults. This is because inverters may experience commutation failures if the AC voltage is below certain threshold [2], [3]. Since most of the HVDC links deliver a very large amount of power, the commutation failure of one single link often induces a severe disturbance to the AC grid, further increasing the risk of cascading faults [4], [5].

In order to reduce the likelihood of commutation failures induced by AC voltage drops, many HVDC links are equipped with commutation failure preventions (CFPREV) [6]. CFPREV is an extinction angle controller that can improve commutation margin by adjusting the inverter firing angle during low voltage periods. The control also leads to greater reactive power consumption, increasing the burden of AC network [7]. As a result, in real world applications CFPREVs need to be carefully tuned.

The associate editor coordinating the review of this manuscript and approving it for publication was Hao Wang.

Traditionally, the impact of controller parameters on HVDC systems are studied through repeated dynamic simulations. However, it is in general not easy to interpret the vast output of simulations, as a result, it is a difficult task to study HVDC control strategies using simulations alone. Besides, the operating models for control design often include uncertain parameters. This situation is becoming worse due to the penetration of renewable sources, resulting in a huge computational burden. A systematic approach for tuning CFPREVs is of interest, both to the practioner and academia.

Several attempts have been reported to cope with the above challenge. Some early results using asymptotic expansion methods were introduced in [8]–[10]. Polynomial approximation based on Galerkin Method was recently introduced in [11]–[13] to deal with parametric problems in power systems. Optimization methods offer a systematic way of tuning system parameters [14], [15], however, they are less transparent as they do not provide much insight. The reason is that optimization methods in general require iterative computations [26], therefore the results they deliver are computational rather than analytical or graphical. It is also difficult to obtain robustness information using an optimization method.

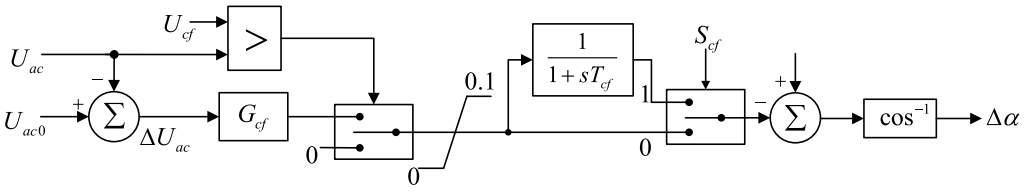


**FIGURE 1.** Diagram of a CFPREV module in electromechanical transient simulation.

In this paper, our recent results [16]–[18] of robust stability analysis are extended to cope with CFPREV parameter tuning. The approach advocated in the work includes two ingredients, these are, rational approximations [19] and value sets. The rational approximations are used to represent the relationship between key performance indices and CFPREVs parameters, while the value sets are employed to unravel the coupling effects of CFPREV parameters by exploiting geometry and graphics.

The rest of the paper is organized as follows: in Section II, the impact of CFPREV on HVDC dynamic performance is introduced and several output variables in AC-DC system are identified as key performance indices. Section III describes the rationale why a rational approximation is preferred. Section IV focuses on solving for the rational approximation problem. In Section V, a multi-index value-set function is established, and the corresponding value set plot is developed. Finally, Section VI shows the effectiveness of the proposed approach as applied to two HVDC systems.

## II. THE IMPACT OF CFPREV ON HVDC DYNAMICS

As is well-known, an inverter valve needs some 300-1000 $\mu$s to gain its forward-blocking capability [1]. If the extinction angle $\gamma$ of an inverter is below the threshold (usually 7° in a 50 Hz system), a commutation failure is unavoidable. In order to reduce the likelihood of the commutation failure induced by voltage drops, many HVDC inverters are equipped with CFPREVs. The diagram of a CFPREV is shown in Fig. 1. As can be seen from the figure, once the commutation voltage $U_{\rm ac}$ drops below the voltage threshold $U_{cf}$, the switch flag $S_{cf}$ will be set to zero and then a correction $\Delta\alpha$ will be added to the computation of firing angle $\alpha_I$ immediately. As a result, the inverter valves will be triggered in advance to increase the commutation margin. Besides, in recovery period, $S_{cf}$ is set to one to include a delay $T_{\rm cf}$ that helps HVDC to recover.

In the sequel, the impact of a CFPREV in a bipolar HVDC link is illustrated. The positive pole of this example is equipped with a CFPREV, while the negative pole is not. Fig. 2 shows the responses of firing angle $\alpha_{\rm I}$ and extinction angle $\gamma$ of two poles. It can be seen that the firing angle of the positive pole is significantly advanced so that the commutation margin increases to successfully avoid a commutation failure, while the negative one experiences a commutation failure.

It is well-understood that, the larger the commutation margin is, the lower the power factor of the inverter is, so the

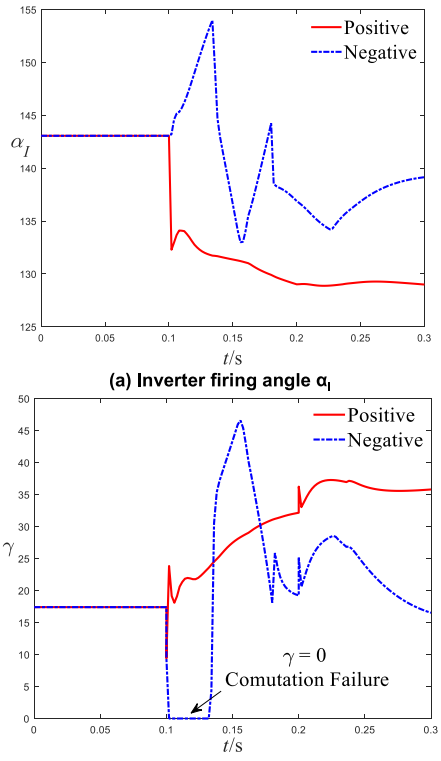


**FIGURE 2.** Simulation results of $\alpha_I$ and $\gamma$ in a bipolar HVDC link ($U_{\rm cf} = 0.85$, $G_{\rm cf} = 0.1$, $T_{\rm cf} = 0.02$s).

inverter absorbs more reactive power from the AC system if CFPREV is activated. Since a CFPREV significantly changes the reactive power characteristics of the inverter, it needs to be carefully designed. To proceed the analysis, here several performance indices are identified, they are: extinction angle $\gamma$, AC voltage amplitude at the inverter terminal, inverter AC voltage dropping rate, and inverter reactive power demand.

## III. PERFORMANCE INDICES AS A FUNCTION OF CFPREV PARAMETERS

In this section we show that the performance indices can be viewed numerically as a rational function of CFPREV parameters. Notice that the dynamics of an AC-DC system is described by the following set of differential-algebraic equations:

$$\begin{cases} \dot{\boldsymbol{x}} = \boldsymbol{f}(\boldsymbol{x}, \boldsymbol{y}, \boldsymbol{p}) \\ \boldsymbol{0} = \boldsymbol{g}(\boldsymbol{x}, \boldsymbol{y}, \boldsymbol{p}), \end{cases} \tag{1}$$

where $\boldsymbol{x}$ denotes state variables, $\boldsymbol{y}$ denotes algebraic variables, $\boldsymbol{p}$ indicates parameter variables such as CFPREVs parameters, $\boldsymbol{f}$ is a vector function representing component dynamics, and $\boldsymbol{g} = \boldsymbol{0}$ represents the usual network equations.

Applying implicit trapezoid integration method to (1), one can obtain the following recursive formula [14]:

$$\begin{cases} \boldsymbol{x}^{k+1} = \boldsymbol{x}^k + 0.5\Delta t[\boldsymbol{f}(\boldsymbol{x}^{k+1}, \boldsymbol{y}^{k+1}, \boldsymbol{p}) + \boldsymbol{f}(\boldsymbol{x}^k, \boldsymbol{y}^k, \boldsymbol{p})] \\ \boldsymbol{0} = \boldsymbol{g}(\boldsymbol{x}^{k+1}, \boldsymbol{y}^{k+1}, \boldsymbol{p}), \end{cases} \tag{2}$$

where $\Delta t$ denotes the integration step-length, $\boldsymbol{x}^k$ and $\boldsymbol{y}^k$ are the results at step $k$, $\boldsymbol{x}^{k+1}$ and $\boldsymbol{y}^{k+1}$ are the results at next step.

The recursive formula constitutes a set of high-dimensional nonlinear algebraic equations about unknown variables, which can be represented in a compact form as

$$\boldsymbol{h}(z, \boldsymbol{p}) = \boldsymbol{0}, \tag{3}$$

where $z$ denotes all the state and algebraic variables, $\boldsymbol{h}$ represents the new algebraic functions.

Assuming that a nominal solution $z_0$ is given, now we are concerned about the effect of uncertainty $\boldsymbol{p}$ on the solution $z$. Using Newton iteration method to solve (3), one obtains the following equations:

$$\boldsymbol{J}(z_0, \boldsymbol{p}) = \partial \boldsymbol{h} / \partial z^{\mathrm{T}} \Big|_{z=z_0}, \tag{4}$$

$$\boldsymbol{J}(z_0, \boldsymbol{p}) z' = \boldsymbol{J}(z_0, \boldsymbol{p}) z_0 - \boldsymbol{h}(z_0, \boldsymbol{p}) = \boldsymbol{b}(z_0, \boldsymbol{p}), \tag{5}$$

where $\boldsymbol{J}$ is the Jacobian matrix, $z$' is the result after the first-iteration and $\boldsymbol{b}$ denotes the right-hand-side vector.

According to *Cramer's Rule*, the $i$-th element of $z$' has an analytical expression as shown below

$$z'_i = \left|\boldsymbol{J}_{(-i)}(z_0, \boldsymbol{p})\right| / |\boldsymbol{J}(z_0, \boldsymbol{p})|, \tag{6}$$

where $|\cdot|$ denotes the determinant, and $\boldsymbol{J}_{(-i)}$ is the result of replacing the $i$-th column of $\boldsymbol{J}$ with $\boldsymbol{b}$.

The above equation shows that $z'_i$ is a rational function of $\boldsymbol{p}$, moreover, the result after subsequent iterations is still a rational function with higher order. As a result, the performance indices selected in the previous section can also be approximated as a rational function of parameter vector $\boldsymbol{p}$.

In the sequel, a two-node test system [20] (see Fig. 3) is used to illustrate the above findings.

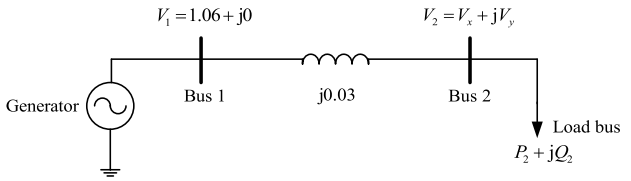


**FIGURE 3.** The two-node test system example.

The nominal solution of the system is as follows: $P_2^{(0)} + jQ_2^{(0)} = 0.5 + j0.3$ and $V_x^{(0)} + jV_y^{(0)} = 1.051 - j0.014$. Considering $P_2$ and $Q_2$ as uncertain parameters, we have:

$$P_2 + jQ_2 = (V_x + jV_y)(1.06 - V_x + jV_y)/(-j0.03). \tag{7}$$

According to (4) - (6), the result of $V_2$ after the 2nd-iteration ($V''_x + jV''_y$) are obtained as follows:

$$\begin{cases} V''_x = \dfrac{0.001(P_2^2 - Q_2^2) + 0.002P_2 + 0.097Q_2 - 1.191}{0.0017P_2 + 0.0611Q_2 - 1.1236} \\ V''_y = \dfrac{-0.00005P_2^2 - 0.002P_2Q_2 + 0.032P_2}{0.0017P_2 + 0.0611Q_2 - 1.1236}, \end{cases} \tag{8}$$

which is clearly a rational fraction.

## IV. DETERMINATION OF RATIONAL APPROXIMATION

### A. ORDER DETERMINATION

Let $\boldsymbol{J}(z_0, \boldsymbol{p})$ in (5) be affine with respect to $\boldsymbol{p}$. Reference [21] points out that an affine matrix $\boldsymbol{L}(\boldsymbol{p})$ with $m$ parameters has the following decomposition:

$$\boldsymbol{L}(\boldsymbol{p}) = \boldsymbol{L}_0 + p_1 L_1 + \ldots + p_m \boldsymbol{L}_m, \tag{9}$$

where $\boldsymbol{L}_i$ is the matrix corresponding to $p_i$.

Let $r_k = rank(\boldsymbol{L}_k)$ be the maximum order of $p_k$ in determinant $|\boldsymbol{L}(\boldsymbol{p})|$. Then the determinant of $\boldsymbol{L}(\boldsymbol{p})$ can be rewritten as:

$$|\boldsymbol{L}(\boldsymbol{p})| = \sum_{i_m=0}^{r_m} \cdots \sum_{i_2=0}^{r_2} \sum_{i_1=0}^{r_1} \alpha_{i_1 i_2 \ldots i_m} p_1^{i_1} p_2^{i_2} \cdots p_m^{i_m}, \tag{10}$$

where $\alpha_{i_1 i_2 \ldots i_m}$ is the coefficient of $p_1^{i_1} p_2^{i_2} \cdots p_m^{i_m}$.

Therefore, the rational approximation expression for a performance index can be expressed as follows:

$$z'_i = \frac{\sum_{i_m=0}^{\bar{r}_m} \cdots \sum_{i_2=0}^{\bar{r}_2} \sum_{i_1=0}^{\bar{r}_1} \bar{c}_{i_1 i_2 \ldots i_m} p_1^{i_1} p_2^{i_2} \cdots p_m^{i_m}}{\sum_{j_m=0}^{r_m} \cdots \sum_{j_2=0}^{r_2} \sum_{j_1=0}^{r_1} c_{j_1 j_2 \ldots j_m} p_1^{i_1} p_2^{i_2} \cdots p_m^{i_m}}, \tag{11}$$

where $\bar{c}$ and $c$ are the monomial coefficients in the numerator and denominator, respectively.

It can be seen from (11) that the maximum order of $|\boldsymbol{L}(\boldsymbol{p})|$ does not exceed the sum of $r_k$, so the maximum order of $z_i$' are also determined. Apparently, the order determined above is exceedingly high even in linear structure and is only of theoretical interest, a more practical solution is required. Fortunately, based on our experience, a simple trial-and-error method turns out to works well. It is also of interest to investigate more advanced order determination instruments (say, [22] and [23]) in the future work.

### B. COEFFICIENT DETERMINATION

Recently, numerical approximation methods have been re-emphasized and advanced in several aspects of power system analysis, and have become powerful complements to traditional simulation methods. The key idea of numerical approximation is to assume that the parametric solution $z(\boldsymbol{p})$ takes a given structure, like polynomial or rational fraction. Once the coefficients in $z(\boldsymbol{p})$ have been determined by numerical methods, an approximate expression for the solution $z(\boldsymbol{p})$ is obtained. In general, polynomial approximation works rather well for many engineering problems. Sometimes,

rational approximation performs better when the function to be approximated is less "flat" [18].

In the sequel, the principle of a numerical approximation method for determining the coefficients in rational function is briefly introduced. Suppose that the index $R$ has a relatively simple rational structure, whose numerator and denominator are 2nd-order multi-linear polynomials (higher-order fractions analogy):

$$R(\boldsymbol{p}) = \frac{\bar{c}_0+\bar{c}_1 p_1+\cdots+\bar{c}_m p_m+\bar{c}_{1,2} p_1 p_2+\cdots+\bar{c}_{m-1,m} p_{m-1} p_m}{c_0+c_1 p_1 \cdots+c_m p_m+c_{1,2} p_1 p_2+\cdots+c_{m-1,m} p_{m-1} p_m}, \tag{12}$$

where $\bar{c}_i$, $\bar{c}_{i,j}$, $c_i$ and $c_{i,j}$ are unknown coefficients.

Substituting sample data into (12) below gives a set of simultaneous linear equations

$$\boldsymbol{X}\boldsymbol{c} = \boldsymbol{y}, \tag{13}$$

where matrix $\boldsymbol{X}$ and column vector $\boldsymbol{y}$ are composed of the sample data and $\boldsymbol{c}$ denotes the vector of unknown coefficients.

Assuming $c_0 = 1$, the coefficient vector $\boldsymbol{c}$ is uniquely determined by the least-square principle.

$$\boldsymbol{c} = \boldsymbol{X}^{+}\boldsymbol{y} = (\boldsymbol{X}^{\mathrm{T}}\boldsymbol{X})^{-1}\boldsymbol{X}^{\mathrm{T}}\boldsymbol{y}, \tag{14}$$

where $\boldsymbol{X}^{+}$ denotes the Moore-Penrose pseudo-inverse of $\boldsymbol{X}$.

It is worth mentioning that the functional relationship between performance indices and parameters determined by the above method only requires a small amount of sample data, and usually has good generalization performance in the overall parametric space. In addition, the impact of some parameters on performance indices can be directly reflected by the corresponding coefficient value in the coefficient vector $\boldsymbol{c}$ (equation (26), for example).

## V. VALUE SET APPROACH FOR MULTI-INDEX ANALYSIS OF HVDC SYSTEM

The numerical approximation procedure described in previous section allows one to obtain expressions that represent the analytical relationship between AC-DC system parameters and performance indices. This section develops a new graphical illustration of the expressions, to further unravel the role each parameter plays.

### A. VALUE SET RESULT OF ONE COMPLEX INDEX

Suppose that the voltage at converter terminal ($\boldsymbol{V}(\boldsymbol{p}) = V_x + \mathrm{j}V_y$ ) has a rational expression obtained from simulation data or measurement data, as shown below:

$$\begin{cases} V_x = N_x(\boldsymbol{p})/D_x(\boldsymbol{p}) \\ V_y = N_y(\boldsymbol{p})/D_y(\boldsymbol{p}), \end{cases} \tag{15}$$

where $N(\boldsymbol{p})$ and $D(\boldsymbol{p})$ are polynomials of appropriate order.

To avoid an inverter commutation failure, $V(\boldsymbol{p})$ should respect the following constraint:

$$V_x^2 + V_y^2 \geq V_{\min}^2, \tag{16}$$

where $V_{\min}$ indicates the critical value of voltage amplitude.

Since $V(\boldsymbol{p})$ is a complex function, the critical condition can be converted into a circle with radius $V_{\min}$ on a complex plane. When $\boldsymbol{p}$ varies in a hyper-box, the variation of $V(\boldsymbol{p})$ forms a value set (or called image set) on the complex plane, as shown in Fig. 4.

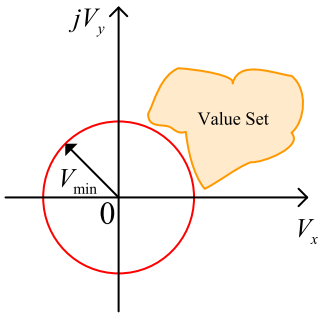


**FIGURE 4.** The value set result and the stability boundary of $V(\boldsymbol{p})$.

The notion of value set is derived from robust stability theory [24]. The idea is to plot the value set of a complex function on a two-dimensional plane. Following the celebrated *boundary crossing theorem* [24], if the value set of the bus voltage $V(\boldsymbol{p})$ lies outside the circle constantly, no commutation failure caused by voltage drops will occur.

While a rational function has certain advantages sometimes, computing its value set is not as straightforward as that of a polynomial. In this work, we construct a new function $\rho_1(\boldsymbol{p})$ called value-set function as follows

$$\rho_1(\boldsymbol{p}) = [N_x(\boldsymbol{p}) - \alpha D_x(\boldsymbol{p})] + \mathrm{j}\left[N_y(\boldsymbol{p}) - \beta D_y(\boldsymbol{p})\right], \tag{17}$$

where $\alpha$ and $\beta$ are real numbers satisfying $\alpha^2 + \beta^2 = V_{\min}^2$.

When the parameters vary in a hyper-box, one obtains a series of value sets of $\rho_1(\boldsymbol{p})$. It is easily understood that the stability criterion $|V(\boldsymbol{p})| = V_{\min}$ is violated if and only if $\rho_1(\boldsymbol{p}) = 0$. This is exactly what *zero-exclusion theorem* [25] claims: the system is stable if and only if the value sets do not intersect the origin. Furthermore, the distance between the value set and the coordinate origin can be viewed as a measure of safety margin (see Fig. 5). In addition, the impacts of each parameter can be read out through the movement of the value sets, see subsequent section for a detailed example.

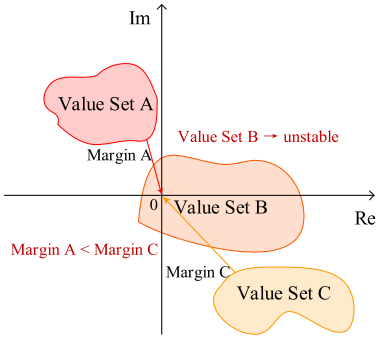


**FIGURE 5.** The value set results of $\rho(\boldsymbol{p})$ and zero-exclusion principle.

It is also convenient to use the angular parameter $\theta \in [0,2\pi]$ to define the value-set function, as shown below:

$$\rho_2(\boldsymbol{p}) = (N_x - D_x V_{\min}\cos\theta) + \mathrm{j}(N_y - D_y V_{\min}\sin\theta), \quad (18)$$

If $\theta$ takes discrete values, a series of value set graphs of $\rho_2(\boldsymbol{p})$ can plotted on the complex plane (see Fig. 6). In Fig. 6, the length of the color map corresponds to the length of the parameter interval, and different colors correspond to the results under different parameter values. It is easily concluded that, if the value sets do not intersect the origin (Fig. 6(a)), then the inverter is under normal operation. On the contrary, if the value sets envelop the origin (Fig. 6(b)), then a commutation failure is likely to occur.

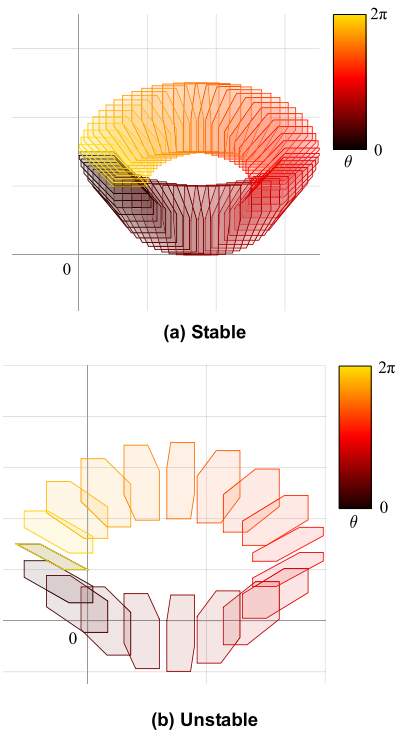


**FIGURE 6.** The value set results of value-set function $\rho_2$.

### B. VALUE SETS OF TWO REAL INDICES

Two indices can also be integrated to produce value set result. For instance, the voltage amplitude and the voltage dropping rate are selected to construct a new value-set function. Suppose the rational expressions of the bus voltage amplitude at two moments $(t_1, t_2)$ are

$$V_{t_1} = N_{t_1}(\boldsymbol{p})/D_{t_1}(\boldsymbol{p}),\ V_{t_2} = N_{t_2}(\boldsymbol{p})/D_{t_2}(\boldsymbol{p});\ V_{t_1} > V_{t_2}. \quad (19)$$

Then the voltage dropping rate is computed by

$$\frac{\Delta V}{\Delta t} = \frac{V_{t_2} - V_{t_1}}{t_2 - t_1} = \frac{N_{t_2}D_{t_1} - N_{t_1}D_{t_2}}{D_{t_2}D_{t_1}(t_2 - t_1)}(\boldsymbol{p}). \quad (20)$$

Considering the operating constraint on the voltage amplitude ($V_t > |V|_{\min}$) and its dropping rate ($\Delta V/\Delta t < R_{\max}$), one obtains the following value-set function:

$$\rho_3(\boldsymbol{p}) = \left[N_{t_2} - D_{t_2}|V|_{\min}\right] + \mathrm{j}\left[D_{t_2}D_{t_1}(t_2 - t_1)R_{\max} - N_{t_1}D_{t_2} + N_{t_2}D_{t_1}\right], \quad (21)$$

The value-set function $\rho_3(\boldsymbol{p})$ is easily applied for operating constraint analysis through its value set result, as shown in Fig. 7.

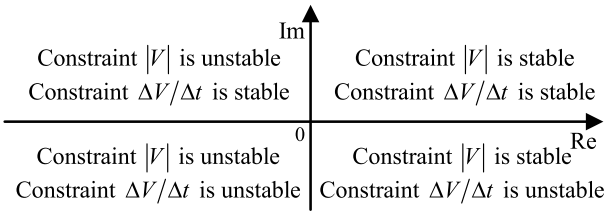


**FIGURE 7.** Operating constraints and value sets.

### C. EXPLOITATION OF VALUE SET GEOMETRY

It is apparent that the number of polynomial terms in a value-set function will increase rapidly as the number of parameters increases. An important observation the value set approach makes use of is that value-set function often enjoys an affine structure or multi-linear structure (i.e., terms like $p_1p_2p_3$). If this is the case, one can have the following elegant result [24]:

1) For an affine value-set function, its value set is a convex polygon with vertices and outer edges all mapped from the vertices and outer edges of the parameter space.
2) For a multi-linear value-set function, its value set is no longer a convex polygon. However, the convex hull of this value set is a convex polygon connected by vertex mapping of the parameter space.

Apparently, if a value-set function is affine, only the vertex mapping needs to be computed. If it is multi-linear, its value set can be quickly estimated through the convex hull formed by the vertex mapping. Only when the convex hull covers the origin, the parameter space needs to be subdivided carefully to calculate the critical value. This is the so-called vertex analysis and it significantly improves computational efficiency. Moreover, if the value-set function is neither affine, nor is it multi-linear, there is still a remedy provided that the number of higher-order polynomial terms is small.

Consider a value-set function like this:

$$\rho_4(\boldsymbol{p}) = (2p_1 + p_1^2)p_2 + \mathrm{j}(p_1^2 + p_2)p_3. \quad (22)$$

The following techniques help to quickly compute the corresponding value sets:

1) Replace the higher-order terms with multi-linear terms using variable substitution. For example, $p_1$ is replaced with the average of two new variables $q_1$ and $q_2$ that have similar variation range. Meanwhile, 2nd-order terms $p_1^2$ is replaced with the product of them. Then (22) is transformed into a multi-linear function as
$$\rho_4'(\boldsymbol{p}) = (q_1 + q_2 + q_1q_2)p_2 + \mathrm{j}(q_1q_2 + p_2)p_3. \quad (23)$$
2) Perform brute force grid computation for $p_1$ only.

### D. MULTI-INDEX-MULTI-PARAMETER ANALYSIS

The value set result is helpful for describing the relationship between system indices and controller parameters. To further enhance the practicability of the value set approach, some plotting techniques suitable for multi-parameter impact analysis are necessary.

1) A series of small value set graphs, which provide more information about system state varying, are drawn by selecting $p_i$ as the key parameter.
2) The movement of the value set graphs, indicated by arrows, reveals the impact of individual parameter on system performance.

The above-mentioned techniques are illustrated by the following example:

$$\rho_5(\boldsymbol{p}) = 1.33(p_1 - p_2 - p_4 - 1) + \mathrm{j}(p_2 - p_3 - p_4 - 1). \tag{24}$$

where $p_1 \in [3, 4]$, $p_2 \in [2, 2.5]$, $p_3 \in [0.5, 0.8]$, $p_4 \in [0, 0.1]$.

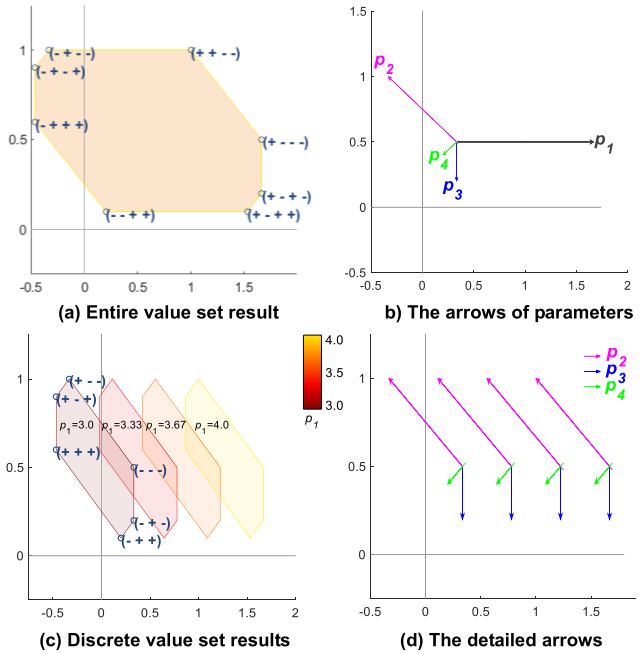


**FIGURE 8.** Multi-parameter value set analysis for $\rho_5(\boldsymbol{p})$.

The entire value set graph is drawn in Fig. 8(a) and the discrete value set graphs under $p_1$ sampling is drawn in Fig. 8(c). In Fig. 8(c), the length of the color map corresponds to the length of the $p_1$, and different colors correspond to the results under $p_1$ taking different values. Besides, the vertexes of the value set are marked with '+' or '−', which represents the upper and lower bounds of each parameter. In Fig. 8(b) and Fig. 8(d), the pointed arrows provide much detailed information about the impact of each parameter on system performance, since their tails and heads are determined through the mapping results of the corresponding parameter extreme values. For instance, the tail and head of the green arrow correspond the mapping results of two parameter configurations $(p_1^-, p_2^-, p_3^-, p_4^-)$ and $(p_1^-, p_2^-, p_3^-, p_4^+)$. This arrow points from Northeast to Southwest, indicating that the increasing of $p_4$ leads to the deterioration of system performance.

A procedure chart summarizing the methods described in the preceding sections is shown in Fig. 9. The key performance indices help us understand the operation status of the system. Then rational approximation establishes the relationship between multiple parameters and the indices. Finally, a value set approach is developed to display the coupling effects of multi-parameters and multi-indices.

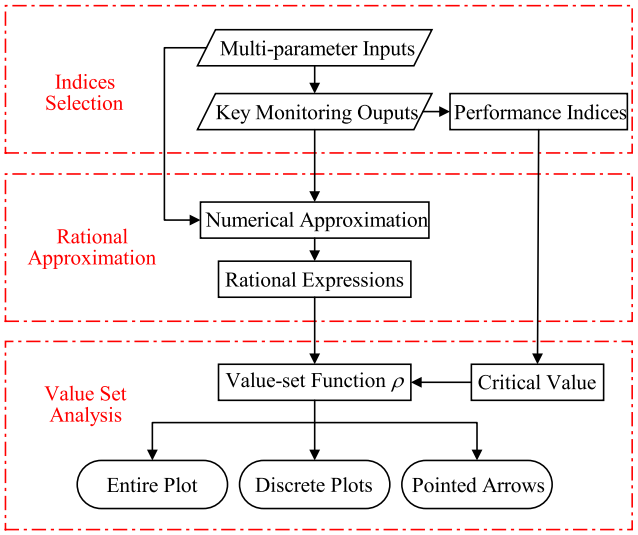


**FIGURE 9.** The procedure chart of the proposed method.

In addition, here are some rule-of thumb guidelines for choosing the order of the rational approximations:

1) If the accuracy requirement is met, the simpler the structure of the approximation expression, the smaller the calculation burden.
2) The simplest case is that the numerator and denominator are both affine polynomials.
3) When the rational approximation adopts the multi-linear structure, the accuracy increases but the computational complexity increases.
4) Gradually increase the highest order of the terms until the accuracy requirement is met or the error is enlarged, and then the order of the rational approximations is determined.

## VI. CASE STUDIES

A small-scale AC-DC system is first utilized to illustrate the efficacy of the rational approximation method and the value set approach. The results of an actual Chinese power system are included later in the section.

### A. A SMALL-SCALE TEST SYSTEM EXAMPLE

The system includes 93 generation units and 7 HVDC links (see Fig. 10). A three-phase short-circuit fault is applied in

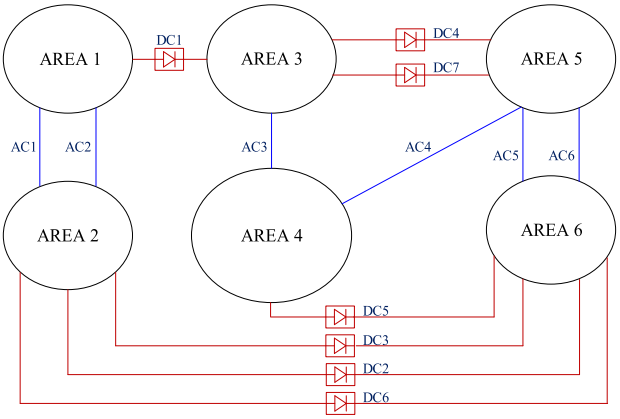


**FIGURE 10.** The structure of the small-scale test system example.

AREA 6, resulting in the voltage drops of converter buses. When the commutation voltages are lower than the threshold $U_{cf}$ (0.85 p.u), the CFPREVs equipped in four HVDC links (DC5, DC3, DC2, DC6) will be activated to regulate.

Here the coupling effects of four gain parameters ($G_{cf}$) in different CFPREVs are analyzed. The parameters vary in the following range: $G_5 \in [0.06, 0.07]$ and $G_3$, $G_2$, $G_6 \in [0.05, 0.15]$. Since DC5 is electrically close to the fault location, the minimum extinction angle of DC5 ($\gamma_{5\min}$) during the fault and the maximum reactive power of DC5 ($Q_{5\max}$) absorbed from the AC system after fault removal are selected as key performance indices.

In order to obtain the data of $\gamma_{5\min}$, the fault line is grounded through small impedance and the commutation failure criterion is disabled. The simulation result shows that $\gamma_{5\min}$ varies from 4.18° to 9.39°, close to the critical value (7°). Using the numerical approximation procedure described in previous sections, the relationship between $\gamma_{5\min}$ and $G_5$, $G_3$, $G_2$, $G_6$ are obtained. In this case, it turns out that the rational approximation results are more accurate than those of polynomial approximations (see Table 1).

**TABLE 1.** The approximation results of $\gamma_{5\min}$.

| Structure | Max-order | MaxAE[a] | MAE[b] | RMSE[c] |
|---|---|---|---|---|
| Multi-linear Polynomial | 1 | 0.5680 | 0.0657 | 0.0886 |
| | 2 | 0.2127 | 0.0442 | 0.0531 |
| | 3 | 0.1546 | 0.0437 | 0.0522 |
| | 4 | 0.1484 | 0.0437 | 0.0522 |
| Rational Fraction | 1 | 0.3187 | 0.0581 | 0.0778 |
| | **2** | **0.0478** | **0.0072** | **0.0098** |

[a] MaxAE means maximum absolute error.
[b] MAE means mean absolute error.
[c] RMSE means root mean square error.

The 2nd-order rational approximation result is as (25).

For the sampling of $Q_{5\max}$, the faulted transmission line is directly grounded and the normal commutation failure criterion is enabled. The simulation result shows that DC5 experiences consecutive commutation failure during the fault and the responses are different only during the recovery. Considering that the maximum reactive power demand of inverter is most affected by its own controller, $G_5$ is selected as the key parameter with a higher degree. In order to obtain more accurate results, it can be assumed that the denominator is only composed of high-order terms of one key parameter to improve the accuracy, while the numerator is still a multi-linear polynomial to maintain computational efficiency. Table 2 below shows the approximation errors.

**TABLE 2.** The approximation results of $Q_{5\max}$ in the given structures.

| Numerator's max-order | Denominator's max-order ($G_5$) | MaxAE | MAE | RMSE |
|---|---|---|---|---|
| 2 | 2 | 3.7864 | 0.5009 | 0.6088 |
| **3** | **2** | **3.2213** | **0.3777** | **0.4789** |
| 3 | 3 | 4.3165 | 1.2303 | 1.5009 |
| 4 | 2 | 3.2182 | 0.3775 | 0.4788 |
| 4 | 3 | 3.7285 | 1.0133 | 1.2299 |

The following expression is the best approximation result, whose numerator is a 3-order multi-linear polynomial and denominator is a 2-order polynomial of $G_5$.

It is seen from (25) and (26), as shown at the bottom of the next page that the coefficients related to $G_2$ and $G_6$ are almost the same, which means these two parameters have the same impact on the system performance. Besides, the sign of the coefficients related to $G_5$ are opposite to the coefficients related to other parameters, indicating that $G_5$ has the opposite impact to other parameters. However, it is difficult to understand the coupling effects of multiple parameters from the above complicated expressions.

Let's see how the value set instrument can help solve this problem. Considering that extinction angle threshold is $\gamma_{CR} = 7°$ and critical reactive power is $Q_{CR} = 170$ MVar, a value-set function is constructed as follows:

$$\rho_{\mathrm{DC5}}(p) = [N_\gamma - D_\gamma \gamma_{CR}] + \mathrm{j}[D_Q Q_{CR} - N_Q]. \quad (27)$$

In Fig. 11(a), the entire value set result of $\rho_{\mathrm{DC5}}$ ($\boldsymbol{p}$) envelopes all quadrants, which shows that improper parameter configuration results in commutation failure and reactive power off-limit simultaneously, while proper one can avoid the situations. Besides, it is remarkable that the arrows in Fig. 11(b) point the impact of each parameter on system performance. This is not only a qualitative result, but also a quantitative one. The arrow representing $G_5$ is longer than others, which indicates $G_5$ is the most important factor. The arrow associated with $G_5$ points from top left to bottom right, indicating that the increase in $G_5$ leads to the consequence that the commutation margin increases, but the voltage of the AC network is deteriorated. Moreover, the value set results also clearly show that $G_2$, $G_3$ and $G_6$ almost uniformly have the opposite impact, because the converter stations of these three links with the same capacity are electrically close to

each other. It is consistent with the conclusion deduced from (25) and (26).

In order to optimize the parameter configuration, a series of discrete value set graphs are drawn by selecting $G_5$ as the key parameter. When $G_5$ is specified, the small value set graphs corresponding parameter subspaces can be quickly obtained by vertex computation, as shown in Fig. 11(c). Through the movement of these small value set graphs, the impact of the key parameter $G_5$ is clearly known. The individual contribution of regular parameters in every small value set is drawn in Fig. 11(d), which also provides useful insights in detail.

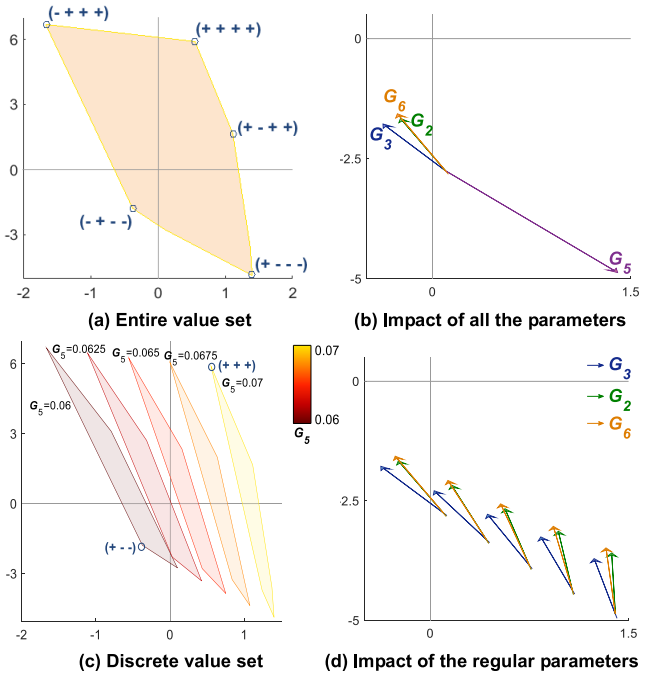


**FIGURE 11.** Value set results of the small-scale test system.

According to the value set results, the best parameter configuration is $G_5 = 0.07$, $G_3 = 0.15$, $G_2 = 0.15$, $G_6 = 0.15$ and the worst is $G_5 = 0.06$, $G_3 = 0.15$, $G_2 = 0.05$, $G_6 = 0.05$. The time-domain simulation results under the above two parameter configurations are compared in Fig. 12.

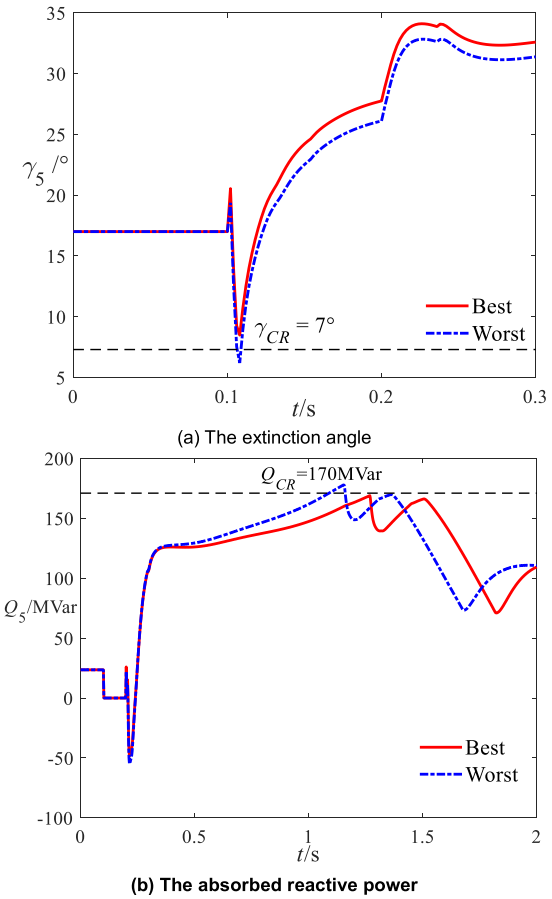


**FIGURE 12.** Time-domain simulation results of the small-scale system.

The result shows that both $\gamma_{5\min}$ and $Q_{5\max}$ under the best parameter configuration are improved, which confirms the validity of the approach.

### B. AN ACTUAL LARGE-SCALE SYSTEM EXAMPLE

The results of applying the proposed approach to an actual Chinese power system with 4441 generation units and 19 HVDC links are reported in this section. In this large-scale grid, Shanghai is a metropolitan area that has 15.7 GW peak load and is powered by five HVDC links. These

$$\gamma_5 = \frac{N_\gamma}{D_\gamma} = \frac{\begin{array}{c}(2 + 20G_5 - 53G_3 - 48G_2 - 48G_6 + 869G_5G_3 + \\ 829G_5G_2 + 807G_5G_6 - 22G_3G_2 - 22G_3G_6 - 23G_2G_6)\end{array}}{\begin{array}{c}(1 - 9.2G_5 - 4.5G_3 - 4G_2 - 4G_6 + 79.7G_5G_3 + \\ 73.8G_5G_2 + 73.6G_5G_6 - 0.3G_3G_2 - 0.2G_3G_6 - 0.6G_2G_6)\end{array}}. \tag{25}$$

$$\begin{aligned} Q_{5\max} = \frac{N_Q}{D_Q} &= \frac{152 + 207G_5 + 33G_3 + 31G_2 + 31G_6}{1 - 1.18G_5 + 8.43G_5^2} \\ &+ \frac{48G_5G_3 + 67G_5G_2 + 60G_5G_6 - 416G_3G_2 - 428G_3G_6 - 406G_2G_6}{1 - 1.18G_5 + 8.43G_5^2} \\ &+ \frac{4335G_3G_2G_6 - 2334G_5G_3G_2 - 2371G_5G_3G_6 - 2821G_5G_2G_6}{1 - 1.18G_5 + 8.43G_5^2} \end{aligned} \tag{26}$$

links are 6.0GW FuFeng HVDC, 2.8GW LinFeng HVDC, 1.1GW GeNan HVDC, 2.9GW YiHua HVDC and 2.9GW LongZheng HVDC, of which the first three and the last two are distributed in two subareas. Considering that Fufeng HVDC link is the largest power source to Shanghai area, the gain coefficient $G_{\mathrm{FF}}$ in its CFPREV module should be concerned carefully. As a result, $G_{\mathrm{FF}} \in [0.015, 0.020]$ is selected as the key parameter and other four gain coefficients ($G_{\mathrm{LF}}$, $G_{\mathrm{GN}}$, $G_{\mathrm{YH}}$, $G_{\mathrm{LZ}} \in [0.05, 0.15]$) are regard as regular parameters.

Then the minimum extinction angle ($\gamma_{\mathrm{FF\_min}}$) of Fufeng HVDC link during a three-phase short-circuit fault and the maximum reactive power consumption ($Q_{\mathrm{FF\_max}}$) of Fufeng HVDC inverter station during the recovery are selected as two performance indices. The results of numerical approximation calculated from simulation data are shown in Table 3 and Table 4.

**TABLE 3.** The approximation results of $\gamma_{\mathrm{FF\_min}}$.

| Structure | Max-order | MaxAE | MAE | RMSE |
|---|---|---|---|---|
| Multi-linear polynomial | 1 | 0.1407 | 0.0663 | 0.0763 |
| | 2 | 0.1263 | 0.0659 | 0.0747 |
| | 3 | 0.1263 | 0.0659 | 0.0747 |
| Rational fraction | **1** | **0.0629** | **0.0169** | **0.0209** |
| | 2 | 1.8825 | 0.0449 | 0.1726 |

**TABLE 4.** The approximation results of $Q_{\mathrm{FF\_max}}$ in the given structures.

| Numerator's max-order | Denominator's max-order ($G_{\mathrm{FF}}$) | MaxAE | MAE | RMSE |
|---|---|---|---|---|
| 2 | 2 | 6.9397 | 1.6534 | 3.4383 |
| **2** | **3** | **2.9183** | **0.8036** | **1.1759** |
| 2 | 4 | 9.8231 | 1.4852 | 3.3514 |
| 3 | 2 | 6.8845 | 1.6548 | 3.4399 |
| 3 | 3 | 2.8920 | 0.8051 | 1.1761 |

By comparing the accuracy of different structures, two excellent expressions for $\gamma_{\mathrm{FF\_min}}$ and $Q_{\mathrm{FF\_max}}$ are determined. The expressions and their critical constraints ($\gamma_{CR} = 7°$ and $Q_{CR} = 3700$ MVar) are used to construct a value-set function. Then value set results of the above value-set function are drawn in Fig. 13.

The movement of the small value set graphs in Fig. 13(a) implies that the larger $G_{\mathrm{FF}}$, the larger the commutation margin of Fufeng HVDC. At the same time, the increase of $G_{\mathrm{FF}}$ causes $Q_{\mathrm{FF\_max}}$ to increase first and then decrease. Moreover, the pointed arrows in Fig. 13(b) unravel the impact of each parameter. It can be seen that the rise of $G_{\mathrm{YH}}$ and $G_{\mathrm{LZ}}$ will reduce the commutation margin of the inverter, but has insignificant impact on the maximum absorbed reactive power. In addition, the increase of $G_{\mathrm{LF}}$ and $G_{\mathrm{GN}}$ has negative impact on two performance indices. Furthermore,

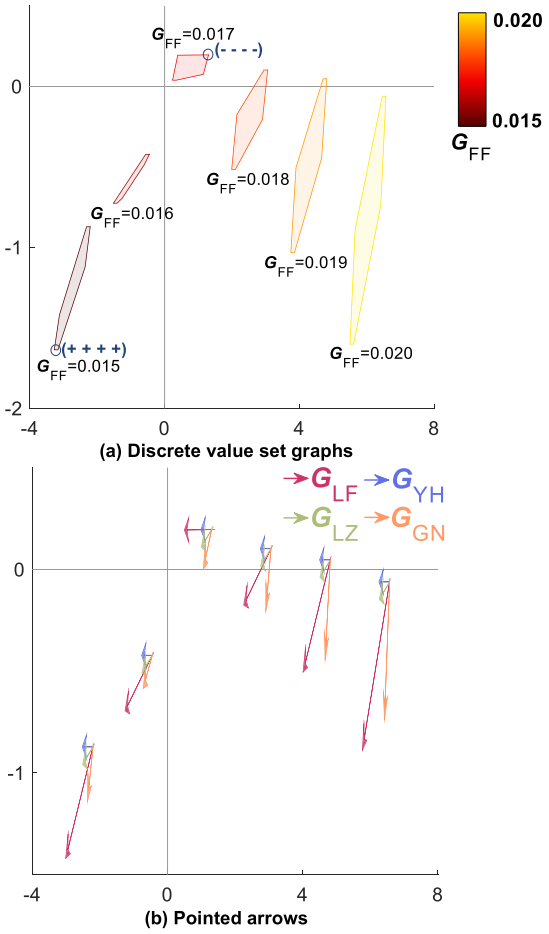


**FIGURE 13.** The value set results of the large-scale actual system.

the difference of the controller parameter impact are also reflected from the length of the arrows in Fig. 13(b).

The results in Fig. 13 are consistent with engineering experience, that is, the converter needs to absorb more reactive power during the recovery once a commutation failure occurs. According to the value set results, the best parameter configuration is determined as $G_{\mathrm{FF}} = 0.017$, $G_{\mathrm{LF}} = 0.05$, $G_{\mathrm{YH}} = 0.05$, $G_{\mathrm{LZ}} = 0.05$, $G_{\mathrm{GN}} = 0.05$ and the worst one is determined as $G_{\mathrm{FF}} = 0.015$, $G_{\mathrm{LF}} = 0.15$, $G_{\mathrm{YH}} = 0.15$, $G_{\mathrm{LZ}} = 0.15$, $G_{\mathrm{GN}} = 0.15$.

In Fig. 14, the time-domain simulation results under the above two configurations are compared. The result shows that $\gamma_{\mathrm{FF\_min}}$ and $Q_{\mathrm{FF\_max}}$ under the best parameter configuration are both improved, which confirms the validity of the introduced approach again.

At the end of this section, we note that the results of the proposed multi-index value set approach can be easily interpreted and provide many insights. Compared with the traditional numerical simulation method, the suggested value set approach yields graphical solutions that unravel the impacts of parameters in CFPREVs on system performance. The approach also considerably improves our early solution [15], which relies heavily on iterative computations.

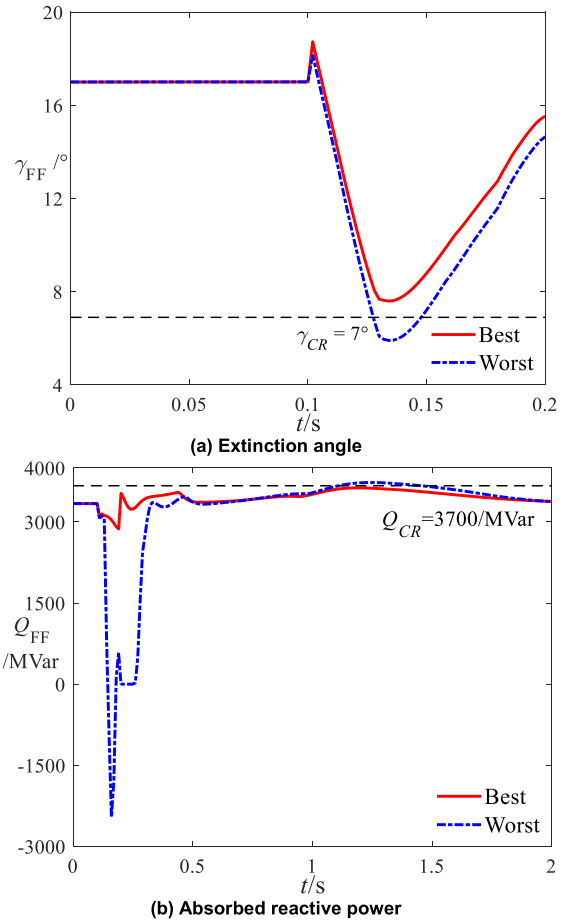


**FIGURE 14.** Time-domain simulation results of the large-scale system.

## VII. CONCLUSION

In this paper, a multi-index value set approach is demonstrated to be a powerful tool for studying HVDC dynamics. Assisted with efficient rational approximations, the proposed value set approach provides a graphical means to unravel the coupling effects of control parameters on HVDC performance indices. The value set graph also allows one to optimize the controller parameter configuration, and conclude that operating constraints are robustly satisfied. As is clear from the paper, the proposed method is sufficiently general, it can also be useful in solving other power system dynamics problems. Moreover, different operating conditions and different fault locations can also be considered as parameters to be analyzed, and their impacts are left as a topic of future research.

## REFERENCES

[1] D. Jovcic and K. Ahmed, *High Voltage Direct Current Transmission: Converters, Systems and DC Grids*. Hoboken, NJ, USA: Wiley, 2015.

[2] Y. Lei, T. Li, Q. Tang, Y. Wang, C. Yuan, X. Yang, and Y. Liu, "Comparison of UPFC, SVC and STATCOM in improving commutation failure immunity of LCC-HVDC systems," *IEEE Access*, vol. 8, pp. 135298–135307, 2020.

[3] Z. Wei, W. Fang, and J. Liu, "Variable extinction angle control strategy based on virtual resistance to mitigate commutation failures in HVDC system," *IEEE Access*, vol. 8, pp. 93692–93704, 2020.

[4] J. Tu, H. Xin, Z. Wang, D. Gan, and Z. Huang, "On self-organized criticality of the east China AC–DC power system—The role of DC transmission," *IEEE Trans. Power Syst.*, vol. 28, no. 3, pp. 3204–3214, Aug. 2013.

[5] L. Li, H. Wu, Y. Song, D. Song, and Y. Liu, "Quantify the impact of line capacity temporary expansion on blackout risk by the state-failure-network method," *IEEE Access*, vol. 7, pp. 183049–183060, 2019.

[6] Z. Wei, Y. Yuan, X. Lei, H. Wang, G. Sun, and Y. Sun, "Direct-current predictive control strategy for inhibiting commutation failure in HVDC converter," *IEEE Trans. Power Syst.*, vol. 29, no. 5, pp. 2409–2417, Sep. 2014.

[7] Y. Xue and X.-P. Zhang, "Reactive power and AC voltage control of LCC HVDC system with controllable capacitors," *IEEE Trans. Power Syst.*, vol. 32, no. 1, pp. 753–764, Jan. 2017.

[8] E. Abed and J. Alexander, "Approximation of faulted power system trjectories via averaging," in *Proc. 26th IEEE Conf. Decis. Control*, Los Angeles, CA, USA, Dec. 1987, pp. 853–865.

[9] N. Duan and K. Sun, "Power system simulation using the multistage adomian decomposition method," *IEEE Trans. Power Syst.*, vol. 32, no. 1, pp. 430–441, Jan. 2017.

[10] G. Gurrala, D. L. Dinesha, A. Dimitrovski, P. Sreekanth, S. Simunovic, and M. Starke, "Large multi-machine power system simulations using multi-stage adomian decomposition," *IEEE Trans. Power Syst.*, vol. 32, no. 5, pp. 3594–3606, Sep. 2017.

[11] B. Xia, H. Wu, Y. Qiu, B. Lou, and Y. Song, "A Galerkin method-based polynomial approximation for parametric problems in power system transient analysis," *IEEE Trans. Power Syst.*, vol. 34, no. 2, pp. 1620–1629, Mar. 2019.

[12] D. Shen, H. Wu, and D. Gan, "Polynomial chaos expansion and its applications in complicated systems with uncertain parameters: A review," *IEEE Syst. J.*, vol. 14, no. 3, pp. 4500–4514, Sep. 2020.

[13] J. R. Hockenberry and B. C. Lesieutre, "Evaluation of uncertainty in dynamic simulations of power system models: The probabilistic collocation method," *IEEE Trans. Power Syst.*, vol. 19, no. 3, pp. 1483–1491, Aug. 2004.

[14] D. Gan, R. J. Thomas, and R. D. Zimmerman, "Stability-constrained optimal power flow," *IEEE Trans. Power Syst.*, vol. 15, no. 2, pp. 535–540, May 2000.

[15] H. Xin, D. Gan, Z. Huang, K. Zhuang, and L. Cao, "Applications of stability-constrained optimal power flow in the east China system," *IEEE Trans. Power Syst.*, vol. 25, no. 3, pp. 1423–1433, Aug. 2010.

[16] J. Zhou, P. Shi, D. Gan, Y. Xu, H. Xin, C. Jiang, H. Xie, and T. Wu, "Large-scale power system robust stability analysis based on value set approach," *IEEE Trans. Power Syst.*, vol. 32, no. 5, pp. 4012–4023, Sep. 2017.

[17] J. Zhou, T. Zheng, and D. Gan, "Value-set-based power system robust stability analysis: Further results," *IEEE Trans. Power Syst.*, vol. 34, no. 2, pp. 1383–1392, Mar. 2019.

[18] P. Shi, J. Zhou, D. Gan, and Z. Wang, "A rational fractional representation method for wind power integrated power system parametric stability analysis," *IEEE Trans. Power Syst.*, vol. 33, no. 6, pp. 7122–7131, Nov. 2018.

[19] P. P. Petrushev and V. A. Popov, *Rational Approximations of Real Functions*. Cambridge, U.K.: Cambridge Univ. Press, 1987.

[20] G. Kusic, *Computer-Aided Power Systems Analysis*. Boca Raton, FL, USA: CRC Press, 2008, pp. 244–250.

[21] S. P. Bhattacharyya, L. H. Keel, and D. N. Mohsenizadeh, *Linear Systems: A Measurement Based Approach*. New Delhi, India: Springer, 2014.

[22] T. Penzl, "A cyclic low-rank smith method for large sparse Lyapunov equations," *SIAM J. Sci. Comput.*, vol. 21, no. 4, pp. 1401–1418, Jan. 1999.

[23] P. Benner, A. Cohen and M. Ohlberger, *Model Reduction and Approximation: Theory and Algorithms*. Philadelphia, PA, USA: SIAM, 2017.

[24] J. Ackermann, *Robust Control: The Parameter Space Approach*, 2nd ed. London, U.K.: Springer-Verlag, 2002, pp. 334–360.

[25] B. R. Barmish, *New Tools for Robustness of Linear Systems*. New York, NY, USA: Maxwell, 1994, pp. 109–122.

[26] M. S. Bazaraa, H. D. Sherali and C. M. Shetty, *Nonlinear Programming: Theory and Algorithms*, 2nd ed. Hoboken, NJ, USA: Wiley, 1993.

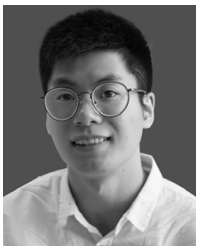

**MINQUAN CHEN** received the B.S. degree in electrical engineering from the College of Electrical Engineering, Zhejiang University, Hangzhou, China, in 2016, where he is currently pursuing the Ph.D. degree. His research interest includes power system stability analysis and control.

**ZHUORAN KANG** received th M.S. degree in electrical engineering with the College of Electrical Engineering, Zhejiang University, China. His research interest includes power system stability analysis and control.

**DEQIANG GAN** (Senior Member, IEEE) received the Ph.D. degree in electrical engineering from Xi'an Jiaotong University, Xi'an, China, in 1994. From 1994 to 1998, he held research positions with Ibaraki University, the University of Central Florida, and Cornell University. From 1998 to 2002, he was with ISO New England, Inc. Since 2002, he has been with the faculty of Zhejiang University, Hangzhou, China. From 2004 to 2006, he visited The University of Hong Kong. From 2007 to 2014, he was an Editor of *European Transactions on Electric Power*. His research interest includes power system stability and control.

**HAO WU** (Member, IEEE) received the Ph.D. degree in electrical engineering from Zhejiang University, Hangzhou, Zhejiang, China. In 2002, he joined Zhejiang University. From 2003 to 2004, he visited The Hong Kong Polytechnic University, and the University of Wisconsin-Madison, from 2009 to 2011. His current research interests include power system operation and stability, uncertainty analysis, cascading failure, load characteristic, and load modeling.